Toward a Robot-Assisted Breast Intervention System

Vishnu Mallapragada, Nilanjan Sarkar, *Senior Member, IEEE*, and Tarun K. Podder, *Member, IEEE*

***Abstract*—Minimally invasive breast biopsies have several advantages, such as low morbidity and decreased cost. However, success of these procedures is critically dependent on precise placement of the biopsy probe at the tumor location. In addition, during manual image-guided breast interventions, freehand ultrasound (US) imaging is challenging and coordinating image acquisition with probe insertion and breast stabilization simultaneously requires high level of skill. To address these problems, a novel robotic breast intervention device is presented in this paper. This system assists the clinician by: 1) ensuring accurate placement of the instrument at the tumor location and 2) autonomously acquiring real-time images of the tumor. Experimental results on breast phantoms demonstrate the efficacy of this device. This system has the potential to increase targeting accuracy while at the same time reducing the level of skill required to perform minimally invasive breast interventional procedures.**

***Index Terms*—Autonomous ultrasound (US) imaging, robot-assisted intervention, tumor manipulation.**

I. Introduction

BREAST cancer is the most common cancer among American women and is the third leading cause of cancer death in women [1]. Approximately 182 000 new breast cancer cases will be diagnosed next year with an estimated death of more than 40 000 women [1]. New minimally invasive procedures such as percutaneous core needle biopsy, radiofrequency ablation, interstitial laser ablation, and cryotherapy offer treatment options that are psychologically and cosmetically more acceptable to patients than traditional surgery [2]. These procedures also have numerous benefits such as low morbidity, decreased cost [3], short operating time, quick recovery of patient, etc.

Early detection of breast cancer has been proven to reduce mortality by about 20%–35% [4]. Histopathological examination is considered to be the "Gold Standard" for definitive diagnosis of cancer, but requires tissue samples that are collected through biopsy. Of the two major approaches for breast biopsy, needle biopsy, and open excisional biopsy, needle biopsy is more attractive because it is less traumatic, produces little or no scar, allows quicker recovery, and is less costly. Despite many benefits of needle biopsy, there are significant technical challenges concerning accurate steering and precise placement of a biopsy needle at the target (in this paper, the word target is used to refer to a tumor, lesion, or just a suspected region of tissue) in the breast. During these procedures, a hollow core needle is percutaneously inserted into the soft, inhomogeneous breast tissue in order to sample a target. In such procedures, it is critical to position the needle tip precisely at the target. Precise placement of the needle at the target is challenging because of several reasons, such as tissue heterogeneity, tissue deformation, target mobility, patient movement, and poor maneuverability of the needle

The current state-of-the-art minimally invasive procedure is highly dependent on the skill of the clinician and requires extraordinary level of hand–eye coordination [5]. Quality discrepancy has been noted in many studies and appears to be related to surgeon volume and/or specific breast surgery or surgical oncology training [6]. It is concluded in [7] that breast-focused surgeons are more competent than the 50% of surgeons who do the occasional case.

To overcome the aforementioned limitations, a new paradigm for image-guided minimally invasive procedures is presented [8], [9]. To demonstrate the efficacy of this paradigm, a novel robot-assisted breast intervention device is developed. Sonography is the most widely used imaging technique because of its real-time capability and cost-effectiveness [10]. Therefore, the robot-assisted breast intervention system presented in this paper is designed for ultrasound (US)-guided percutaneous breast biopsy. The biopsy instrument used for experimental validation is a 10-gauge vacuum-assisted hollow core biopsy needle. The specific subsystems of this device are as follows. 1) *A robotic manipulation mechanism:* a mechanism to compensate for needle–target misalignment for providing access to mobile targets. 2) *A US imaging system:* an image acquisition system for dynamic tracking of the location of a target in real time using a 2-D US probe. These two subsystems are then integrated for a semiautomated modality of breast interventions. This device will potentially enhance clinical efficacy of image-guided breast interventions.

The rest of the paper is organized as follows. Section II presents the design of the robotic system. Section III describes the overall control architecture of the system. Section IV presents experimental results on breast phantoms (soft plastic material that mimics breast tissue). Section V summarizes the conclusions of this paper.

II. System Design

A. Design of a Robotic Manipulation Mechanism

Currently available commercial biopsy instruments do not compensate for target movement. Freehand US-guided biopsy

Manuscript received September 1, 2009; revised November 25, 2009 and April 6, 2010; accepted May 18, 2010. Date of publication September 23, 2010; date of current version September 7, 2011. Recommended by Technical Editor D. Stoianovici.

V. Mallapragada is with Stryker Medical, Kalamazoo, MI 49048 USA (e-mail: vishnu.goutham@gmail.com).

N. Sarkar is with the Departments of Mechanical Engineering and Computer Engineering, Vanderbilt University, Nashville, TN 37235 USA (e-mail: nilanjan.sarkar@vanderbilt.edu).

T. K. Podder is with the Department of Radiation Oncology, Thomas Jefferson University, Philadelphia, PA 19107 USA (e-mail: tarun.podder@jeffersonhospital.org).

Color versions of one or more of the figures in this paper are available online at http://ieeexplore.ieee.org.

Digital Object Identifier 10.1109/TMECH.2010.2068575

and stereotactic biopsy are the most common techniques for sampling breast tissue. Freehand US-guided biopsies are typically performed with the patient in a supine position. During the procedure, clinicians simultaneously 1) manipulate the target position (by applying force on the breast using fingers) and stabilize the breast; 2) steer and insert the needle; and 3) manipulate US probe for imaging needle and target while monitoring the US image screen continuously.

Stereotactic biopsy, on the other hand, is typically performed with the patient in a prone position. Needle insertion and target sampling are guided by X-ray imaging, which is a nonreal-time imaging modality. Breast is stabilized by compressing it between two plates. This helps to reduce target movement to some extent. However, since the tissue is deformable, target movement is not eliminated and leads to sampling errors and multiple needle insertions.

Several researchers have designed robotic systems to improve the accuracy of needle insertions [11]–[16]. The reader is referred to [11] for a detailed review of state of the art in interventional robotic systems. A significant research effort is being focused to investigate techniques that can address the problem of target movement during needle insertion. In [17] and [18], steerable devices are presented that allow the clinician to steer the tip of the needle toward the target during insertion. A visually controlled needle-guiding system is developed in [19] for automatic- or remote-controlled percutaneous interventions. In [20] and [21], a finite-element model is used to predict movement of the target.

In contrast to these existing techniques, we approach the problem from an opposite viewpoint. We employ "target manipulation," where multiple robotic fingers autonomously manipulate the tissue externally to position a target inline with the needle during insertion based on image feedback from a US probe. Breast tissue is inhomogeneous and its biomechanical properties are nonlinear. Hence, tissue deformation displaces the target from its original location during needle insertion. Robotic fingers positioned around the breast apply force on the surface of the breast based on the image of the target to guide the target toward the line of insertion of the needle. The system can autonomously position a target at a desired location (typically in the path of the needle) with a high degree of accuracy.

To determine the number of robotic fingers and their geometric arrangement necessary for planar position control of a target embedded inside the deformable object, we use the force closure theorem [9] in mechanics: 1) at least three robotic fingers are required; and 2) the arrangement of the fingers should be such that the end points of their force direction vectors draw a nonzero triangle that includes their common origin point. With such an arrangement, the target position can be controlled in a plane.

The robotic image-guided breast intervention system presented here is designed for prone position breast interventions. Prone position offers maximum workspace with good surface contact area on the breast for the robotic fingers. Needle incision site and orientation of the needle are chosen by the clinician considering factors, such as location of target, location of critical anatomical structures, and ease of access to target. The desired target position is the point where the line of insertion (of the needle) intersects the plane containing the target. While one can choose any plane that contains the target and has an intersection with the line of needle insertion, this plane is chosen to be the horizontal plane for simplicity. The desired target position is determined by a planner (see Section III) based on the actual target location and needle orientation. Note that planar (horizontal plane) target position control is sufficient to be able to successfully position the target along the line of insertion of the needle.

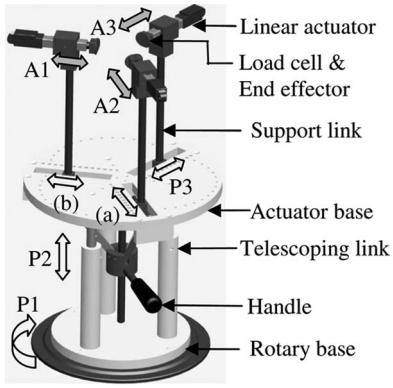

Fig. 1. Manipulation mechanism with three DoF and three DoA.

The overall design requirements for the manipulation mechanism are as follows.

1) As earlier discussed, planar manipulation of deformable objects requires three robotic fingers with a geometric arrangement such that the end points of their force direction vectors draw a nonzero triangle that includes their common origin point.
2) Design should facilitate easy access to needle guidance system and US imaging system.
3) Force applied by the fingers should be limited to avoid injury to the patient.
4) Mechanism should be adjustable to accommodate different breast sizes.
5) Mechanism should be compact.
6) Mechanism should be inexpensive.

Based on these requirements, a manipulation mechanism is designed, as shown in Fig. 1. In Fig. 1, clear block arrows represent passive degrees of freedom (DoF) and shaded block arrows represent degrees of actuation (DoA).

The system consists of a rotary base that rotates about the central vertical axis (P1). The rotary base has a detent locking mechanism that can be used to lock the entire system at eight different positions (45° intervals). The actuator base is connected to the rotary base with three telescoping links. The telescoping links can be used to move the actuator base vertically (P2). These links provide a range of motion of 122 mm. The telescoping links can be fixed using a locking pin. These two DoF provide flexibility in positioning the system for convenient access based on location of the target and needle incision site.

The robotic finger for applying force on the breast consists of a lead-screw-driven linear actuator, an end-effector, and a load cell. The miniature linear actuator (L12-50-210-12-P, Firgelli Technologies, Inc.) is a dc-motor-driven lead screw with a gear ratio of 210:1. They are lightweight (weight 37 g, dimensions 18 mm $\times$ 15 mm $\times$ 115.5 mm) having a stroke of 50 mm and a force capability of 45 N (at a speed of 2.5 mm per second). The end-effector is a contoured link that can apply compressive, frictionless force on the breast. A load cell (MSP6948-ND, Digikey) is mounted between the end-effector and the linear actuator to measure the force applied by the finger. Three fingers (A1, A2, and A3) are positioned 120° apart to satisfy conditions for planar target position control. The direction vectors of the three fingers (with respect to a global coordinate frame) are n_1, n_2, and n_3, respectively.

The finger mechanisms are mounted on support links that are attached to sliders underneath the actuator base. A handle can be used to move the center coupler vertically. Vertical motion of the center coupler is transformed into coordinated radial motion (P3, P4, and P5) of the sliders through the connecting links. Radial motion of the fingers is used to accommodate different breast sizes. The finger mechanisms can be moved 100 mm radially.

The robotic fingers have a cylindrical workspace of 2209 cm^3 (12.5 cm height and 7.5 cm radius). The system has a footprint of 2027 cm^2 and an overall height of 49 cm. It has three DoA (A1, A2, and A3) and three DoF (P1, P2, and coupled P3, P4, and P5). The mechanism is compact and its open structure facilitates easy positioning and access for needle guidance system and US imaging system. The mechanism is designed using off-the-shelf components to minimize cost.

B. Design of a US Imaging System

One of the limitations of US-based imaging is that the US probe has to be continuously in contact with the surface of the breast to ensure acoustic coupling. Force sensors are typically used to ensure contact between the tissue surface and the US probe during image-guided robotic medical procedures [22]–[24]. Even though these systems greatly reduce the difficulty of acquiring US images, the target cannot be tracked in real time if it moves out of the imaging plane of the probe. In [25], a speckle decorrelation technique for estimating out-of-plane motion of a target is presented. This approach assumes rigid motion of internal tissue to preserve correlation between successive image planes. Due to needle insertion and robotic manipulation, large tissue deformation occurs inside the breast, which limits application of this technique.

We design a system for autonomous positioning of the US probe that can dynamically track the location of a target inside the breast. The design requirements for this system are as follows.

1) The system should be developed for a 2-D US probe that is currently used for US-guided breast interventions.
2) It should maintain contact between the US probe and the surface of the breast for acoustic coupling.
3) It should have the ability to move the US probe in a 2-D plane that is perpendicular to the imaging plane of the probe to recapture the target image if the target deflects away from the original imaging plane.

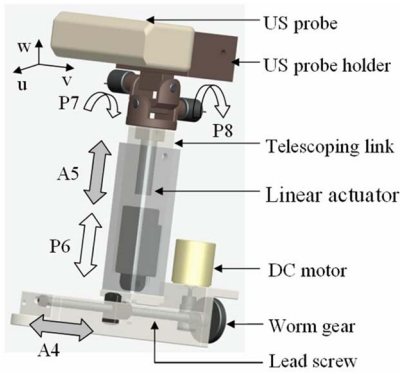

Fig. 2. Autonomous US image acquisition device with three DoF and two DoA.

4) It should be compact.

Based on these requirements, a design for the autonomous image acquisition system is developed, as shown in Fig. 2. In Fig. 2, clear block arrows represent passive DoF and shaded block arrows represent DoA.

The US probe is mounted on an end-effector that has two DoF (P7 and P8). The imaging plane of the US probe is the u–v plane. The end-effector can rotate about u (P7, range of motion 69°) and v (P8, range of motion 70°) axes for orienting the US probe such that the imaging plane is parallel to the needle. The end-effector is driven using a two DoF Cartesian robot. Vertical motion (A5) is achieved using a lead-screw-driven linear actuator. The miniature linear actuator (L12–30-210–12-P, Firgelli Technologies Inc) is a dc-motor-driven lead screw with a gear ratio of 210:1. The actuator is lightweight (weight 37 g, dimensions 18 mm $\times$ 15 mm $\times$ 95.5 mm) having a stroke of 30 mm and a force capability of 45 N with a maximum speed of 2.5 mm per second. The actuator is mounted inside a telescoping link that provides additional adjustability in vertical positioning of the US probe (P6, range of motion 42 mm). This mechanism is mounted on a slide that is moved using a lead screw mechanism for horizontal motion (A4, range of motion 55 mm). The lead screw mechanism is driven using a dc motor (no load speed 7800 r/min, maximum torque 5 mNm; 2224012SR, Micromo Electronics, Inc.) with a worm gear drive (reduction ratio 45:1; S1C83Z-P048B090D, SDP/SI).

If the US probe is not in contact with the breast, the US probe is moved along A4 to make contact with the breast. The system can also slide the US probe using the linear actuator (A5) for tracking the location of a target if it moves out of the imaging plane (u–v). US gel (clear-image high-viscosity US gel, Cone Instruments) is used for coupling between the US probe and the phantom. The gel also acts as a lubricant for smooth sliding along the surface. This system has two DoA (A4 and A5) and three DoF (P6, P7, and P8). All joint coordinates are measured using rotary and linear potentiometers.

C. Design of a Needle Guidance System

The aforementioned two subsystems, i.e., the manipulation mechanism and the US imaging subsystems, are independent of a needle guidance system, but in order to carry out

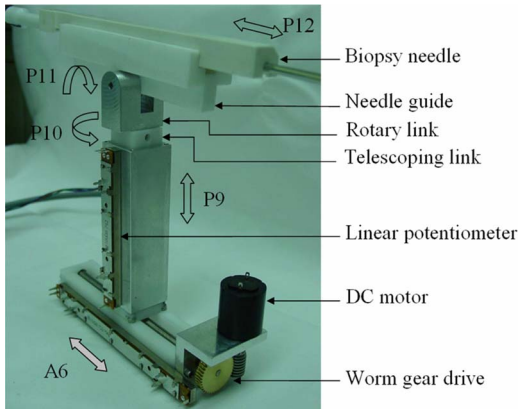

Fig. 3. Needle guidance system with four DoF and one DoA.

experimentation, we needed to design a needle guidance system (see Fig. 3). Fig. 3 shows a needle guidance platform that facilitates orientation of the needle based on location of the target and other critical anatomical structures. The system has four DoF (P9, P10, P11, and P12) and one DoA (A6). All joints of the system are equipped with potentiometers for determining the needle orientation. Essentially, this platform is capable of orienting the needle to reach any target in the breast.

The needle guide provides linear guidance (P12) for inserting the needle into the breast. The needle guide is mounted on a rotary link and can rotate (P11, range of motion 57°) about the horizontal axis perpendicular to the needle. The rotary link is attached to a telescoping link and rotates (P10, range of motion 50°) about a vertical axis. The telescoping link can be moved vertically (P9, range of motion 55 mm) to adjust the height of the needle. This mechanism is mounted on a lead-screw-driven actuator for automated positioning (A6, range of motion 63 mm) of the needle at the desired incision site. Note that the needle guidance system facilitates manual needle insertion, which is under the direct control of the clinician. Also note that the needle guidance system is not used to steer the needle. Needle–target alignment is ensured only through target manipulation. The needle guidance system facilitates positioning of the needle based on the incision site and direction of insertion chosen by the clinician. In this regard, needle trajectory can be chosen anywhere by the clinician.

D. Integrated System

Fig. 4 shows the integrated robotic breast intervention system. The manipulation mechanism, US imaging system, and needle guidance system are integrated in such a manner that the complete robotic system is compact. The US imaging system and the needle guidance system are mounted on the actuator base (see Fig. 1). The actuator base has slots that are 120° apart for accommodating radial movement of the fingers. Both the US imaging system and the needle guidance system can passively rotate (P14 and P13 in Fig. 4(c), respectively; range of motion 110°) about the vertical axes and thus can be placed at any angle (current configuration shows in steps of approximately 8°) between two adjacent fingers of the manipulation mechanism. The global reference frame is located on the vertical axis passing through the center of the actuator base. The rotation of the US imaging system and needle guidance system is measured by rotary potentiometers mounted on the actuator base. As a result, transformation matrices determine the position of the image plane (u–v plane in Fig. 2) and the needle orientation with respect to the global reference frame. Frame assignment and transformation matrices for determining orientation of US image plane and needle are presented in [26].

The integrated system shown in Fig. 4 has six actuated DoF. Three (A1, A2, and A3 in Fig. 1) for the manipulation mechanism, two for the US imaging system (A4 and A5 in Fig. 2), and one for the needle guidance device (A6 in Fig. 3). The system has 14 potentiometers for measuring position coordinates of all the links. Three potentiometers measure the extension of the robotic fingers (A1, A2, and A3 in Fig. 1), five potentiometers measure joint coordinates of the US imaging system (A4, A5, P6, P7, and P8 in Fig. 2), and four potentiometers measure joint coordinates of the needle guidance system (A6, P9, P10, and P11 in Fig. 3). Three load cells measure the force applied by the robotic fingers (see Fig. 1). A 16-channel, 16-bit analog input board (PCI-DAS6034, Measurement Computing) is used for reading the analog data for input to the control algorithm. Analog data are sampled at a rate of 1 KHz. An 8-channel, 16-bit analog output board (PCI-DDA08/16, Measurement Computing) is used for controlling the fingers. To overcome friction-generated limit cycle behavior, pulse position modulation (PPM) is used to control the actuators. Therefore, the duty cycle is the actuator input. A timer chip (NE555, Texas Instruments) generates the PPM signal for driving a full-bridge driver (L298, ST Microelectronics) that controls the actuators.

Image frames from the US unit (Eccocee SSA-340 A, Toshiba) are sent to a computer (1.6 GHz and 2 GB RAM) in RS-170 format. Image frames are digitized using a frame grabber card (DT3120, Data Translation) and an image processing algorithm extracts position coordinates of the target. The image processing algorithm consists of the following steps: 1) region segmentation to extract the region of interest; 2) histogram equalization; 3) thresholding to differentiate the target from the background; 4) median filtering to remove noise; and 5) blob analysis to extract target centroid coordinates. Target position data are communicated serially to a microcontroller (Freescale 68HC912B32, 8 MHz clock frequency). The microcontroller outputs this data in a 16-bit parallel format. This data are read by another computer (1.6 GHz and 1 GB RAM) using a data acquisition card (PCIM DDA06/16, Measurement Computing). One iteration of image processing and data communication requires a maximum time of 0.2 s. This is the time delay in the feedback loop of the controller. This computer runs the control algorithm and outputs control signals to the motor driver circuit for driving the robotic fingers.

The robotic system is designed with the following safety features to avoid catastrophic failure or accidental injury during operation: 1) all mechanical components of the system are designed to ensure structural safety; 2) robotic fingers have built in overload protection so that if the force exceeds 45 N, actuator shuts off to prevent injury; 3) robotic fingers have built in limit

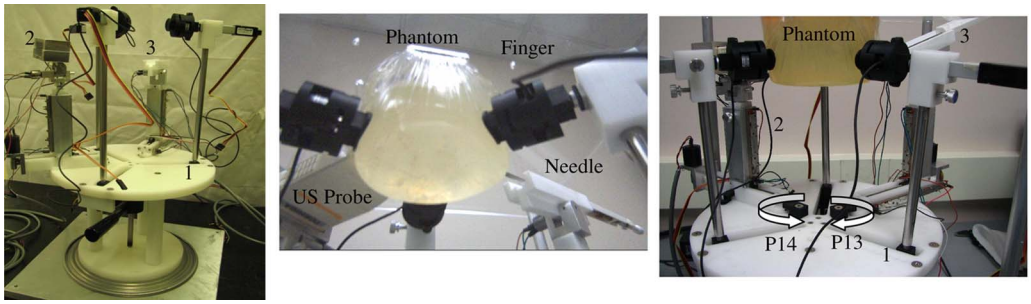

Fig. 4. Robotic image-guided breast intervention system. (a) 1—Manipulation mechanism; 2—US image acquisition system; and 3—needle guidance system. (b) (Bottom view) Phantom suspended vertically from the top. Image shows robotic fingers, US probe, and needle in contact with the phantom for a needle insertion. (c) (Side view) Image shows two additional DoF for US imaging system and needle guidance system.

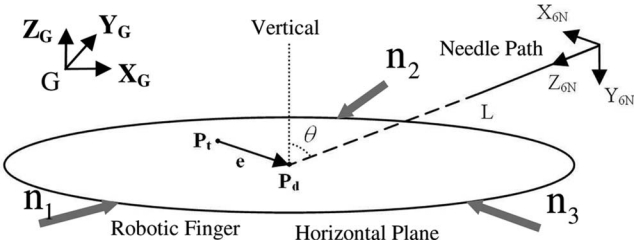

Fig. 5. Needle–target alignment during breast intervention. The horizontal plane passing through the target represents a cross section of the breast.

switches to avoid over compression; 4) range of motion of the fingers is also limited through software control; and 5) a panic button is integrated into the system for manual shut down in case of emergency.

III. Control Architecture

The control architecture for the robotic system consists of low-level controllers for the manipulation mechanism and the US imaging system integrated through a high-level supervisory controller. In the current system, needle insertion is performed manually using the needle guidance device.

A. Controller for Robotic Manipulation Mechanism

1) Planner: Fig. 5 shows a schematic of needle orientation and target position during breast intervention. $\mathbf{P_t}$ (letters in bold represent vectors) is the actual target position, $\mathbf{P_d}$ is the desired target position, and $\mathbf{e}$ is the error vector (these are 2-D vectors measured with respect to the global reference frame). It can be observed from the schematic that the desired target position is along the needle path.

To facilitate ease of positioning of the robotic fingers, horizontal plane is chosen for manipulation. Note that we only need to control the target position in two dimensions (e.g., horizontal plane) to be able to successfully position it along the line of insertion of the probe. It is, however, possible for the target to move out of the initial horizontal plane. Ideally, one would need to move the actuators to contain the target in a parallel horizontal plane. However, in general, we will not need to move the actuators due to two reasons. First, typically the target deflection is small [27] (e.g., in our experimental trials with many phantoms, we never experienced more than 10 mm target deflection). When the force is applied through surface contact (as opposed to point contact) such deflection can be accommodated. Second, there exists kinematic coupling between the contact point and the target point in the breast due to the continuity of the medium (breast tissue). Therefore, the actuators are located in the horizontal plane initially containing the target. The desired target position is at the point of intersection of the needle path and the horizontal plane. Therefore, the error vector is also located in the horizontal plane. Altitude (θ) indicates the angle between needle and the vertical. The needle is inserted at an angle to the horizontal plane to have a unique intersection point ($\theta \neq 90^\circ$). $\mathrm{C_{6N}}$ (defined by axes $X_{6\mathrm{N}}Y_{6\mathrm{N}}Z_{6\mathrm{N}}$) is the coordinate frame attached to the needle. L is the distance between the origin of the needle coordinate frame and the desired target position.

The transformation between the needle coordinate frame and the global reference frame is given by ${}^{\mathrm{G}}_{6}\mathrm{T_N}$. Let

$$ {}^{\mathrm{G}}_{6}\mathrm{T_N} = \begin{bmatrix} r_{11} & r_{12} & r_{13} & P_x \\ r_{21} & r_{22} & r_{23} & P_y \\ r_{31} & r_{32} & r_{33} & P_z \\ 0 & 0 & 0 & 1 \end{bmatrix} \tag{1} $$

where r_{ij}, P_x, P_y, and P_z are elements of the transformation matrix. The desired target position with respect to the global reference frame is defined as

$$ {}^{\mathrm{G}}\mathbf{P_d} = [x_{td} \quad y_{td} \quad z_t \quad 1]^T \tag{2} $$

where x_{td} and y_{td} are the desired target position coordinates. z_t is the Z coordinate of the actual target position in the global reference frame. Let ${}^{6}\mathbf{P_d}$ denote the desired target position (in 3-D coordinates) with respect to the needle frame

$$ {}^{6}\mathbf{P_d} = [0 \quad 0 \quad L \quad 1]^T \tag{3} $$

since the desired target position is at a distance L along $Z_{6\mathrm{N}}$ (see Fig. 5). The desired target position with respect to the global reference frame is, ${}^{\mathrm{G}}\mathbf{P_d}$, given by

$$ {}^{\mathrm{G}}\mathbf{P_d} = {}^{\mathrm{G}}_{6}\mathrm{T}^{6}_{\mathrm{N}}\ \mathbf{P_d}. \tag{4} $$

Substituting from (1) and (3), we have

$$ {}^{\mathrm{G}}\mathbf{P_d} = [\, r_{13}L + P_x \quad r_{23}L + P_y \quad \bar{\mathrm{r}}_{33}L + P_z \quad 1\,]^T. \tag{5} $$

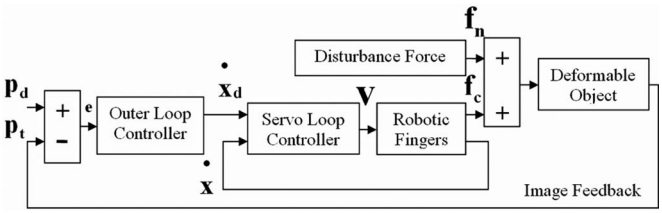

Fig. 6 Control structure for the manipulation mechanism.

Equating the third element of ${}^{\mathrm{G}}\mathbf{P_d}$ from (3) and (6), we have

$$L = \frac{z_t - P_z}{r_{33}}. \tag{6}$$

As discussed earlier, $\theta \neq 90^\circ$; therefore, $r_{33} \neq 0$. Equating the first and second elements of ${}^{\mathrm{G}}\mathbf{P_d}$ from (2) and (5), we have

$$x_{td} = r_{13}L + P_x \tag{7}$$

$$y_{td} = r_{23}L + P_y \tag{8}$$

where x_{td} and y_{td} are the desired target coordinates given to the low-level controller of the manipulation mechanism for positioning the target along the needle path.

2) Target Position Control: The target position error $\mathbf{e}$ is

$$\mathbf{e} = \mathbf{P_d} - \mathbf{P_t}. \tag{9}$$

Fig. 6 shows a schematic of the controller of three robotic fingers in contact with the breast that guides a target from any point $\mathbf{P_t}$ to an arbitrary point $\mathbf{P_d}$ within the breast.

The low-level controller for the manipulation mechanism is similar to the proportional integral (PI) controller presented in [8]. In this paper, this controller is improved by the addition of an inner servo loop to add damping to the system. In Fig. 6, the target position data are obtained through image feedback. The desired target position is determined by the planner based on the current target location and the needle path. The desired target position is always along the line of insertion of the needle. Error vector $\mathbf{e}$ is the difference between the desired and the actual target position. An outer loop controller determines the desired velocity for the actuators (which drive the robotic fingers) $\dot{\mathbf{x}}_\mathbf{d}$ depending on the target position error (P control). A servo loop controller (PI controller) acts on the error between the desired and actual actuator velocities $\dot{\mathbf{x}}$ to generate the actuator input **v.** The desired control objective can be achieved with just the outer loop controller; the inner servo loop is used to add damping to the system [28]. The actuator velocities are determined using approximate differentiation of the position signals. The actuators drive the robotic fingers to apply a controlled external force $\mathbf{f_c}$ on the surface of the object to guide the target toward the desired position. The control loop mitigates the effect of an external disturbance force $\mathbf{f_n}$ on the target position.

B. Controller for US Imaging System

The controller for the US image acquisition system consists of two subsystems. The first subsystem is used to track the target position in 3-D, and the second subsystem is used to ensure contact between the US probe and the breast surface.

1) Target Tracking: Tracking the location of a target (3-D coordinates) using a 2-D US probe requires knowledge of the position of the probe and coordinates of the target in the image plane of the probe. Potentiometers are used to measure the orientation of the probe. Coordinates of the target are extracted using an image processing algorithm (described in Section II-D), if the target is in the imaging plane. The presence of the target in the image plane is inferred when blob analysis (during image processing) detects the target in the image frame. If the target is out of the imaging plane, there is uncertainty in determining the location of the target with respect to the imaging plane, i.e., there is no information regarding the location of the target in a direction perpendicular to the imaging plane. In such a case, a search strategy exhaustively searches for the target using a position-controlled linear actuator. The linear actuator (A5 in Fig. 2) moves the US probe in a direction perpendicular to the image plane along a desired trajectory x_{5d} given by

$$x_{5d} = A\sin\left(2\pi f\left(t - t_0\right)\right) \tag{10}$$

where A is the amplitude (7.5 mm), f is the frequency (1/15 Hz), and t_0 is the time (in seconds) at which target tracking is enabled.

In the interval $[t_0\ t_0 + 3.75]$, the US probe is moved vertically (perpendicular to the image plane) upwards. If during this time the target is detected, the actuator stops moving to keep the target in the image plane. If the target is not detected by moving along this direction, the actuator reverses and moves along the opposite direction in the interval $(t_0 + 3.75 t_0 + 11.25]$ to locate the target. Since typically the target movement is not greater than 10 mm, by moving the US probe 7.5 mm in each direction vertically (total 15 mm), the target should be detected. A proportional controller is used to track the desired trajectory. If for any reason, the target is not found, then the aforementioned cycle is repeated until the target is detected.

2) Contact Detection: Due to high acoustic impedance of air, the US probe has to be in contact with the breast for imaging the target and surrounding tissue. Surface deformation due to robotic manipulation and needle insertion may result in the US probe losing contact with the breast. The region in the image close to the edge (where the US probe makes contact with the surface) is used to detect the contact state of the US probe. This region is extracted from the US image and Otsu's method [29] is used to estimate the gray-scale threshold for the region. When the probe is in contact with the surface, the threshold is small and when the probe breaks contact with the surface, the threshold increases. This change in the threshold is used to infer the contact state of the probe. During an interventional procedure if the probe breaks contact with the breast, the US probe is moved radially inwards (along A4 in Fig. 2) using the linear actuator (P control) to reestablish contact.

C. Hybrid Supervisory Controller

A supervisory controller is used to integrate the controllers of the US imaging system and manipulation mechanism. It monitors and coordinates these two controllers based on discrete events. A detailed description of the hybrid supervisory controller is presented in [30].

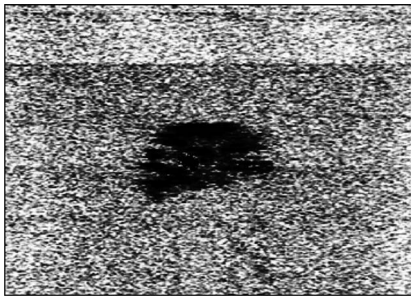

Fig. 7. US image of target in phantom. Dark blob in the image is the target.

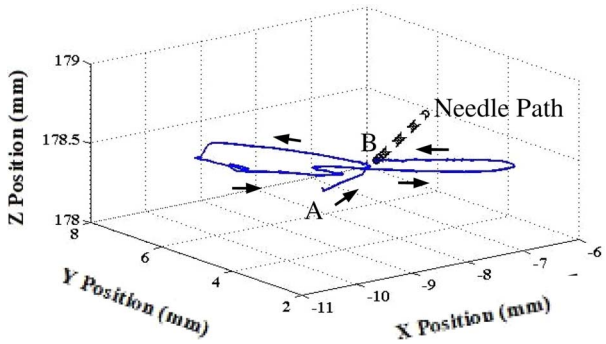

Fig. 8. Target and nominal needle paths during needle insertion.

IV. Experimental Results

A. Needle Orientation in Global Reference Frame

In these experiments, a needle is aligned with the target using the needle guidance system based on eye-approximation and then joints of the needle guidance device are locked. Based on the proprioceptive measurements, needle path is computed. The computed needle path is used in (1) for target manipulation. Due to sensor inaccuracy and mechanical limitations, the actual needle path may be slightly different from the computed needle path. In the future, needle path may be dynamically determined by using a 6-DOFs electromagnetic (EM) sensor (for instance miniBIRD from Ascension Tech has translational and angular accuracy of 1.8 mm and 0.5°, respectively), which also facilitates freehand needle insertion.

B. Experimental Setup

Deformable plastic phantoms are built in such a manner that their material properties closely resemble breast tissue properties, as published in the literature [31]. Breast tissue properties vary greatly based on factors, such as age, presence of tissue abnormality, etc. In order to demonstrate the feasibility of this technique under significant parameter variation, phantoms are prepared with varying elastic properties to demonstrate that the controller can work in realistic scenarios. Details about phantom preparation and elastic properties of the phantom material can be found in [32]. A target (plastic insert) is embedded inside the phantom during the molding process to mimic a tumor/lesion. Fig. 7 shows the target in an image frame grabbed from the US machine.

The experimental setup is shown in Fig. 4(b). The phantom is suspended vertically (to mimic prone patient position) and the needle is inserted into the phantom using the needle guidance system. A 10-gauge (approximate diameter 2.5 mm) hollow core needle is used for this experiment. In this experimental setup, the US probe is coplanar (horizontal plane) with the robotic fingers. A needle is inserted at an angle (altitude θ) to the horizontal plane. Therefore, needle insertion is not parallel to the image plane of the US probe. The US probe is placed coplanar with the robotic fingers because the thickness of the image slice obtained with the US probe is about 5 mm. Therefore, the maximum resolution (in controlled coordinates, X and Y) of target position is obtained when the image plane is coplanar with the target manipulation plane (horizontal plane).

Unit vectors defining the direction of force application by the robotic fingers are n_1, n_2, and n_3. In this setup,

$$n_1 = [0.5 \;\; 0.866], \quad n_2 = [0.5 \;\; -0.866], \quad n_3 = [-1 \;\; 0]. \tag{11}$$

1) Experiment 1 (Minimizing Needle–Target Misalignment During Needle Insertion): This experiment demonstrates the efficacy of this system in minimizing needle–target misalignment during needle insertion. An inhomogeneous phantom (see [32] for details) with an embedded target is used in this experiment. In Fig. 8, point A is the initial location of the target and point B is the final location of the target. It can be observed from Fig. 8 that the target is not located on the needle path initially (point A).

Robotic fingers apply external force to minimize the initial misalignment. As the needle is inserted (altitude 70°), due to disturbance force exerted by the needle (first puncture occurs at point A*), target moves out of the needle path. The robotic fingers compensate for the random target movement and steer the target onto the needle path (point B). Fig. 9 shows a plot of the X and Y coordinates of the target position. It can be observed from Fig. 9 that needle insertion and target manipulation takes about 30 s. At the end of needle insertion, the target is positioned at the needle tip accurately. In this experiment, the US probe is continuously in contact with the phantom and the target remains in the image plane of the probe.

2) Experiment 2 (Target Tracking During Needle Insertion): This experiment demonstrates the efficacy of the supervisory controller in coordinating the manipulation mechanism and US imaging system. A homogeneous phantom with an embedded target is used in this experiment.

Fig. 10 shows the target and needle paths during 3-D needle insertion. In Fig. 10, point A is the initial location of the target. It can be observed from Fig. 10 that the target is not located on the needle path initially (point A). As the needle is inserted (altitude 60°), manipulation mechanism applies external force to minimize needle-target misalignment. An external disturbance (simulating vertical patient movement) is applied at point B, which results in the target moving out of image plane of the US probe. At point B, out-of-plane target movement is detected (through segmentation of the US image) and the manipulation mechanism is disabled by the supervisory controller.

Fig. 11 shows the target position response along X and Y coordinates. From point B, target position data are not

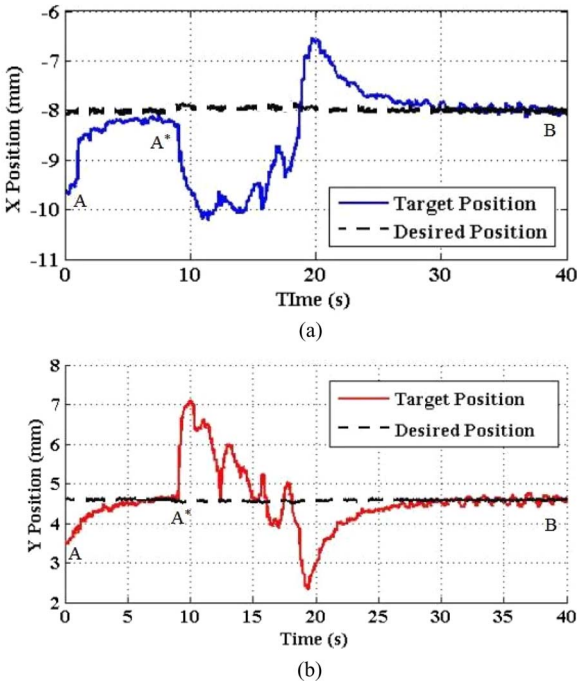

Fig. 9. Target position response during needle insertion. (a) X displacement. (b) Y displacement.

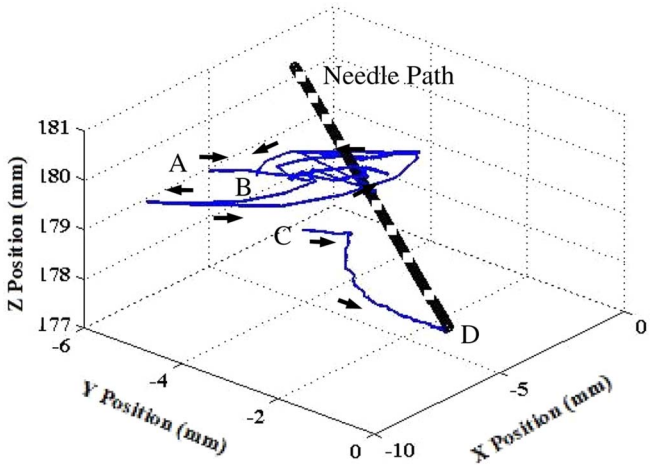

Fig. 10. Target and nominal needle paths during 3-D needle insertion.

available since the target is not identified in the US image. The needle insertion is stopped when the manipulation mechanism is disabled, since target deflection is not compensated due to unavailability of target position coordinates. At point B, the supervisorycontroller enables target tracking. The US probe is moved [along trajectory defined by (10)] using the US imaging system to search and recover the target. Fig. 12 shows the movement of the US probe along the prismatic joint (A5 in Fig. 2) of the US device. At point C, the target is detected and the supervisory controller shifts the control back to the manipulation mechanism. At this point, needle insertion is resumed. From point C, robotic fingers steer the target toward the needle path. At the end of needle insertion, the target is positioned at the needle tip accurately (point D). It can be observed from Fig. 11 that

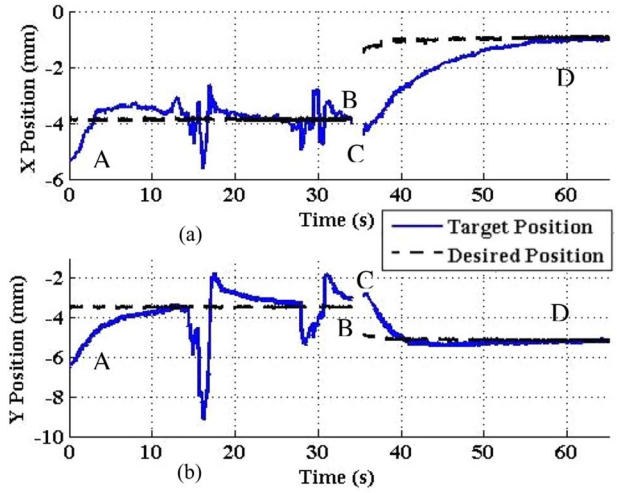

Fig. 11. Target position response with target tracking during needle insertion. (a) X displacement. (b) Y displacement.

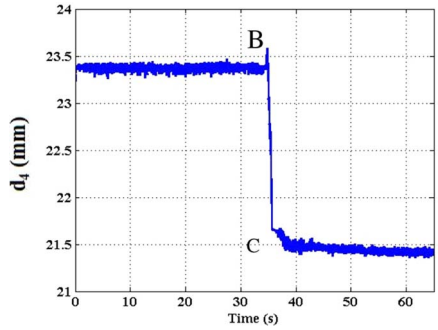

Fig. 12. Joint coordinate of US image acquisition device.

needle insertion and coordinated probe movement with robotic manipulation takes about 62 s.

C. Targeting Accuracy

Targeting accuracy is defined as the error between the centroid of the target and the needle axis when the needle is in a prefire position. In the aforementioned experiments, steady state is the prefire position of the needle. Steady state indicates that the needle is positioned close to the target and is ready to be fired for sampling or ablating the target. The root mean square error (RMSE) is used to quantify targeting accuracy. RMSE is defined as

$$\text{RMSE} = \sqrt{\frac{\sum_{t=t_i}^{t_f} (\mathbf{P_n} - \mathbf{P_t})^2}{n}} \tag{12}$$

where $\mathbf{P_n}$ is a point on the needle axis such that a line passing through $\mathbf{P_n}$ and $\mathbf{P_t}$ is perpendicular to the needle axis. Table I shows the RMSE values for 13 trials. Since targeting accuracy is evaluated at steady state, t_i and t_f are chosen such that the time interval spans the last 5 s of the experiment. Sampling time for the controller is 0.001 s, hence n equals 5001. It can be observed from Table I that the 1) average error in target position is 0.17 mm (minimum 0.02 mm and maximum 0.40 mm) and 2) average time taken for positioning the target at the needle

TABLE I
TARGETING ACCURACY

Trial	Phantom	Needle Altitude (degrees)	RMSE (mm)	Time (s)
1	1 (H)	10	0.04	37
2	1 (H)	10	0.37	35
3	1 (H)	20	0.13	40
4	1 (H)	15	0.23	30
5	1 (H)	20	0.07	38
6	2 (H)	30	0.02	62
7	2 (H)	20	0.07	42
8	5 (I)	20	0.08	35
9	5 (I)	10	0.40	45
10	5 (I)	20	0.33	40
11	5 (I)	20	0.12	25
12	5 (I)	20	0.16	20
13	5 (I)	20	0.14	32

I—Inhomogeneous and H—homogeneous.

tip is 37 s (minimum 20 s and maximum 62 s). Note that the error in target position is one order less than the needle diameter ($\sim$2.5 mm).

It is to be noted that accuracy is also dependent on the resolution of the US images. After digitizing the US images with the frame grabber card, the pixel size is 0.19 mm (for a US depth setting of 8.0 cm). Therefore, an error of atleast $\pm$0.10 mm exists in determining the target centroid. Resolution can be improved by reducing the depth setting on the US machine. However, there is a tradeoff between resolution and depth of imaging.

V. CONCLUSION

A novel device for image-guided minimally invasive breast interventions has been presented. The basic concept is to use robotic fingers to manipulate the position of a target embedded in soft tissue for minimizing needle–target misalignment. This is a novel approach that is fundamentally different from techniques presented so far in literature that rely on needle steering or finite-element analysis for path preplanning. The potential advantages of this approach are increased success rate, reduced patient discomfort, and enhanced diagnostic outcome. Experimental results on phantoms indicate good accuracy in target positioning. This system can be used to quickly and accurately sample a target with a single insertion during breast interventions. Experimental results demonstrate that this system is capable of autonomously tracking a target in 3-D space using a 2-D US probe. Discussion with several breast surgeons and radiologists indicate that such a system will have utility in hospitals without dedicated breast centers, where highly skilled breast surgeons are not available.

As with any system, there are some limitations, which are as follows. 1) Target position information is derived through segmentation of US images. Though it is possible to segment US images of phantoms, real-time segmentation of breast US images is more challenging. 2) To maximize the resolution of target position coordinates, the US probe is arranged coplanar with the target manipulation plane. Hence, the needle and the US image plane are not parallel. This may present difficulty to a clinician in identifying the needle tip before sampling the target. 3) Although in all our experiments with significantly varying phantom properties, we did not observe any needle bending, in other procedures where smaller diameter needles are used such as fine needle aspiration, bending of needle may be an issue. Using a 6-DoF EM sensor is the ideal choice for determining the needle path. In such a case, the needle tip and the target position are known accurately. Therefore to aid the clinician, needle and target positions can be rendered on a visual display. This can give the clinician visual confirmation before sampling the target.

Future work will include CT validation, development of visual display of needle path, and animal phantom study using the enhanced robotic system. Subsequently, we will apply for IRB approval to use the system for human subjects.

ACKNOWLEDGMENT

The authors would like to thank all the Radiologists, Breast Surgeons, and Breast Oncologists who provided feedback about the presented robotic system. In particular, they would like to specially thank K. McManus, A. Chakravarthy, and I. Meszoely, for their insightful discussions during the course of this research.

REFERENCES

[1] American Cancer Society (ACS). (2009, Feb.) *Cancer Facts & Figures* [Online]. Available: http://www.cancer.org/downloads/STT/2008CAFFfinalsecured.pdf

[2] G. Vlastos and H. M. Verkooijen, "Minimally invasive approaches for diagnosis and treatment of early-stage breast cancer," *Oncologist*, vol. 12, no. 1, pp. 1–10, 2007.

[3] M. Cross, "Minimally invasive breast biopsy: A new standard in the new millenium," in *Proc. Semin. Breast Disease: Radiol., Pathol. Surg. Considerations*, 2004, vol. 7, no. 4, pp. 148–152.

[4] J. G. Elmore, K. Armstrong, C. D. Lehman, and S. W. Fletcher, "Screening for breast cancer," *J. Amer. Med. Assoc.*, vol. 293, no. 10, pp. 1245–1256, Mar. 2005.

[5] B. D. Fornage and B. S. Edeiken, "Percutaneous ablation of breast tumor," in *Tumor Ablation: Principles and Practice*. New York: Springer-Verlag, 2005, pp. 428–439, ISBN 13:978-0387-95539-1.

[6] K. A. Skinner, J. T. Helsper, D. Deapen, W. Ye, and R. Sposto, "Breast cancer: Do specialists make a difference?" *Ann. Surg. Oncol.*, vol. 10, pp. 606–615, 2003.

[7] H. A. Pass, S. V. Klimberg, and E. M. Copeland, "Are "breast-focused" surgeons more competent?" *Ann. Surg. Oncol.*, vol. 15, no. 4, pp. 953–955, 2008.

[8] V. Mallapragada, N. Sarkar, and T. Podder, "Robot assisted real-time tumor manipulation for breast biopsy," in *Proc. IEEE Int. Conf. Robot. Autom.*, 2008, pp. 2515–2520.

[9] V. Mallapragada, N. Sarkar, and T. Podder, "Robot assisted real-time tumor manipulation for breast biopsy," *IEEE Trans. Robot.*, vol. 25, no. 2, pp. 316–324, Apr. 2009.

[10] L. Liberman, T. L. Feng, D. D. Dershaw, E. A. Morris, and A. F. Abramson, "US-guided core breast biopsy: Use and cost-effectiveness," *Radiology*, vol. 208, pp. 717–723, 1998.

[11] K. Cleary, A. Melzer, V. Watson, G. Kronreif, and D. Stoianovici, "Interventional robotic systems: Applications and technology state-of-the-art," *Minimally Invasive Ther. Allied Technol.*, vol. 15, no. 2, pp. 101–113, 2006.

[12] N. V. Tsekos, J. Shudy, E. Yacoub, P. V. Tsekos, and I. G. Koutlas, "Development of a robotic device for MRI-guided interventions in the breast," in *Proc. Bioinf. Bioeng. Conf.*, 2001, pp. 201–208.

[13] D. Stoianovici, L. Whitcomb, J. Anderson, R. Taylor, and L. Kavoussi, "A modular surgical robotic system for image guided percutaneous procedures," in *Proc. MICCAI* (Lecture notes in Computer Science, vol. 1496), 1998, pp. 404–410.

[14] K. Cleary,M. Freedman, M. Clifford, D. Lindisch, S. Onda, and L. Jiang, "Image-guided robotic delivery system for precise placement of therputic agents," *J. Controlled Release*, vol. 74, no. 1, pp. 363–368, Jul. 2001.

[15] A. Patriciu, S. Solomon, L. Kavoussi, and D. Stoianovici, "Robotic kidney and spine percutaneous procedures using a new laser-based CT registration method," in *Proc. MICCAI*, 2001, vol. 2208, pp. 249–257.
[16] D. Stoianovici, J. A. Cadeddu, R. D. Demaree, S. A. Basile, R. H. Taylor, L. L. Whitcomb, W. N. Sharpe, Jr., and L. R. Kavoussi, "A novel mechanical transmission applied to percutaneous renal access," in *Proc. ASME Dyn. Syst. Control Division (DSC)*, 2001, vol. 61, pp. 401–406.
[17] S. Okazawa, R. Ebrahimi, J. Chuang, S. E. Salcudean, and R. Rohling, "Hand-held steerable needle device," *IEEE/ASME Trans. Mechatronics*, vol. 10, no. 3, pp. 285–296, Jun. 2005.
[18] R. J. Webster III, J. S. Kim, N. J. Cowan, G. Chirikjian, and A. M. Okamura, "Nonholonomic modeling of needle steering," *Int. J. Robot. Res.*, vol. 25, no. 5/6, pp. 509–526, May/Jun. 2006.
[19] M. H. Loser and N. Navab, "A new robotic system for visually controlled percutaneous interventions under CT fluoroscopy," in *Proc. MICCAI* (Lecture Notes in Computer Science, vol. 1935), 2000, pp. 887–896.
[20] F. S. Azar, D. N. Metaxas, and M. D. Schnall, "Methods for modeling and predicting mechanical deformations of the breast under external perturbations," *Medical Image Anal.*, vol. 6, pp. 1–27, 2002.
[21] R. Alterovitz, K. Goldberg, J. Pouliot, R. Taschereau, and I.-C. Hsu, "Sensorless planning for medical needle insertion procedures," in *Proc. IEEE Int. Conf. Intell. Robots Syst.*, Oct. 2003, pp. 3337–3343.
[22] F. Pierrot, E. Dombre, E. Degoulange, L. Urbain, P. Caron, S. Boudet, J. Gariepy, and J. Megnien, "Hippocrate: A safe robot arm for medical applications with force feedback," *Med. Image Anal.*, vol. 3, no. 3, pp. 285–300, 1999.
[23] A. Vilchis, J. Troccaz, P. Cinquin, K. Masuda, and F. Pellisier, "A new robot architecture for tele-echography," *IEEE Trans. Robot. Autom.*, vol. 19, no. 5, pp. 922–926, Oct. 2003.
[24] P. Abolmaesumi, S. E. Salcudean, W. Zhu, M. R. Sirouspour, and S. P. DiMaio, "Image-guided control of a robot for medical ultrasound," *IEEE Trans. Robot. Autom.*, vol. 18, no. 1, pp. 11–23, Feb. 2002.
[25] A. Krupa, G. Fichtinger, and G. D. Hager, "Full motion tracking in ultrasound using image speckle information and visual servoing," in *Proc. IEEE Int. Conf. Robot. Autom.*, 2007, pp. 2458–2464.
[26] V. Mallapragada, "Towards a robot assisted breast biopsy system," Ph.D. dissertation, Dept. Mech. Eng., Vanderbilt Univ., Nashville, TN, 2008.
[27] S. P. DiMaio and S. E. Salcudean, "Needle insertion modeling and simulation," *IEEE Trans. Robot. Autom.*, vol. 19, no. 4, pp. 864–875, Oct. 2003.
[28] D. Alazard and J. P. Chretien, "Flexible joint control: Robustness analysis of the collocated and non-collocated feedbacks," in *Proc. IEEE Int. Conf. Intell. Robots Syst.*, 1993, pp. 2102–2107.
[29] N. Otsu, "A threshold selection method from gray-level histograms," *IEEE Trans. Syst., Man, Cybern.*, vol. SMC-9, no. 1, pp. 62–66, Jan. 1979.
[30] V. Mallapragada, N. Sarkar, and T. Podder, "Autonomous coordination of imaging and tumor manipulation for robot assisted breast biopsy," in *Proc. IEEE/RAS-EMBS Int. Conf. Biomed. Robot. Biomechatron.*, Oct. 2008, pp. 676–681.
[31] P. Wellman, "Tactile imaging," Ph.D. dissertation, Div. Eng. Appl. Sci., Harvard Univ., Cambridge, MA, 1999.
[32] V. Mallapragada, N. Sarkar, and T. Podder, "A robotic system for real-time tumor manipulation during image guided breast biopsy," in *Proc. IEEE Int. Conf. Bioinf. Bioeng.*, 2007, pp. 204–210.

Vishnu Mallapragada received the B.Tech. degree from the Indian Institute of Technology, Chennai, India, the M.S. degree from North Carolina State University, Raleigh, and the Ph.D. degree from Vanderbilt University, Nashville, TN, all in mechanical engineering.

He is currently with Stryker Medical, Kalamazoo, MI. His research interests include biomedical robotics, mechatronics, and control systems.

Nilanjan Sarkar (S'92–M'93–SM'04) received the Ph.D. degree in mechanical engineering and applied mechanics from the University of Pennsylvania, Philadelphia, and received Postdoctoral training at Queen's University, Kingston, ON, Canada.

He is currently an Associate Professor in the Departments of Mechanical Engineering and Computer Engineering, Vanderbilt University, Nashville, TN. He was an Assistant Professor at the University of Hawaii before joining Vanderbilt University. His research interests include the areas of robotics, control, and human–robot interaction.

Dr. Sarkar has served as an Associate Editor for the IEEE TRANSACTIONS ON ROBOTICS.

Tarun K. Podder (S'99–A'01–M'04) received the M.E. degree in mechanical engineering from the Indian Institute of Science, Bengaluru, India, in 1990, and the Ph.D. degree in robotics and automation from the University of Hawaii at Manoa, Honolulu, in 2000.

From 1990 to 1991, he was a Research Engineer at the Robotics and Mechatronics Centre, Indian Institute of Technology, Kanpur, India. From 1991 to 1997, he was a Lecturer in the Department of Mechanical Engineering, University of Calcutta, Calcutta, India. From 2001 to 2006, he was a Research Scientist at Rochester Institute of Technology, a Research Specialist and Project Manager at RSystems, Inc., a Research Fellow at Monterey Bay Aquarium Research Institute, and a Research Assistant Professor at the University of Rochester. He is currently an Assistant Professor in the Department of Radiation Oncology, Thomas Jefferson University, Philadelphia, PA. His research interests include system dynamics, path planning and control of robotic and autonomous systems, medical robotics, and robot-assisted radiation therapy.

Dr. Podder is a member of the American Society of Mechanical Engineers, the IEEE Engineering in Medicine and Biology Society, the IEEE Robotics and Automation Society, the American Association of Physicists in Medicine, and the American Society for Therapeutic Radiology and Oncology.